Journal of Organometallic Chemistry, *478* (1994) 141–151

The effects of back-bonding to phosphines on the *trans* influence in $[Mo(NH)Cl_3(PR_3)_2]^{0,\pm 1}$ (R = H, Me and F)

Paul D. Lyne [a] and D. Michael P. Mingos [b]

[a] *Inorganic Chemistry Laboratory, South Parks Road, Oxford, OX1 3QR (UK)*
[b] *Department of Chemistry, Imperial College of Science, Technology and Medicine, South Kensington, London, SW7 2AY (UK)*

(Received October 27, 1993)

Abstract

Approximate density Functional Theory calculations were used to study the *trans* influence in $[Mo(NH)Cl_3(PR_3)_2]^{0,\pm 1}$ (R = H, Me and F) complexes. The geometries of the complexes have been fully optimized in the C_{2v} point group. The extent of the lengthening of the bond between the metal and the *trans* chloride relative to the *cis* chlorides appears to diminish as the electronic occupation of the molybdenum d orbitals is increased from d^0 to d^2. In addition, the angular distortion of the *cis* ligands away from the imido group also decreases as the metal d orbital occupation increases. These findings are in agreement with structural characterization of related complexes. The reason for the structural changes in these complexes has been identified as back-bonding from the metal to the phosphine σ^* orbitals in the d^2 complexes. The d^2 electrons reside in a molecular orbital that is bonding with respect to metal–phosphine interactions, and anti-bonding with respect to metal–*cis* chloride interactions. The angular distortion is kept to a minimum in the d^2 complexes in order to maximize the overlap between the metal d_{xy} orbital and the phosphine σ^* orbitals. As a consequence the metal–*cis* chloride bonds lengthen. The bonding energies between the $[Mo(NH)Cl_3]^-$ and $(PR_3)_2$ fragments have been calculated. The extent of back-bonding to the phosphines has been determined to be greatest when the phosphine is PF_3. Inclusion of d polarization in the phosphorus basis set slightly increases the extent of back-bonding to the phosphines.

Key words: Molybdenum; Imido complexes; Phosphine; Molecular orbital calculations; *Trans*-influence; Density fluctional theory

1. Introduction

Transition metal imido complexes have received particular attention owing to their importance in many diverse areas, including synthetic [1–3], metabolic [4] and industrial processes [5]. A characteristic feature of the geometries of octahedral imido complexes is the presence of a *trans* influence [6–10]. This *trans* influence manifests itself as a lengthening of the metal–ligand bond *trans* to the imido group. Additionally, in six-coordinate complexes, the ligands *cis* to the imido group tend to bend away from it to give a distorted pseudooctahedral structure (see Fig. 1). A similar *trans* influence has been noted for other complexes with axial stereochemistry containing multiply bonded ligands such as imido, nitrido and oxo.

Wilkinson *et al.* [11] have published the structures of a series of organoimido tungsten complexes in the IV, V and VI oxidation states. In particular the authors presented structural results for $[W(NR)Cl_2(PR'_3)_3]^+$ and $[W(NR)Cl_2(PR'_3)_3]$. Both of these complexes were

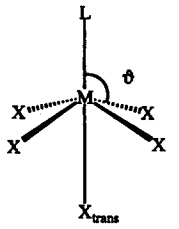

L = N, O, NR

θ > 90°: Typically θ = 94° - 98°

M-X_{trans} longer than M-X_{eq}

Fig. 1. Illustration of the *trans* influence in six-coordinate octahedral complexes.

Correspondence to: Professor D.M.P. Mingos.

0022-328X/94/$7.00
SSDI 0022-328X(93)24305-O

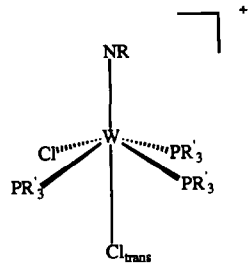

$W\text{-}Cl_{trans}$ = 244.3pm
$W\text{-}Cl_{eq}$ = 238.2pm
W-P = 259.0pm

1

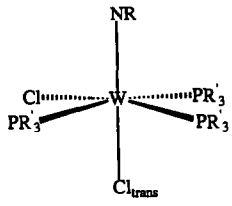

$W\text{-}Cl_{trans}$ = 250.1pm
$W\text{-}Cl_{eq}$ = 249.1pm
W-P = 247.7pm

2

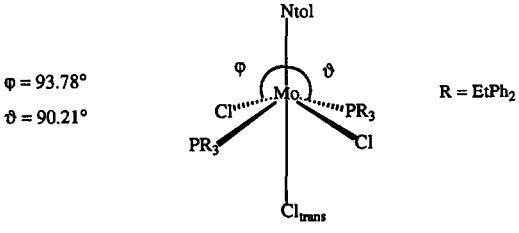

φ = 93.78°
ϑ = 90.21°

R = $EtPh_2$

$Mo\text{-}Cl_{trans}$ = 248.6pm
$Mo\text{-}Cl_{eq}$ = 238.7pm

Mo-P = 259.9pm
Mo-N = 172.5pm

3

found to have a pseudooctahedral structure with a *cis mer* configuration (see **1** and **2**).

Despite the configurational similarities of these two complexes, they appear to differ significantly in the extent of the *trans* influence exerted by the imido group on the *trans* chloride ligand. In the d^1 complex, $[W(NR)Cl_2(PR'_30_3]^+$, the *trans* chloride has a bond length to tungsten that is 10 pm longer than the $W\text{-}Cl_{eq}$ bond. However, in the d^2 complex the $W\text{-}Cl_{trans}$ bond is actually shorter than the $W\text{-}Cl_{eq}$ bond by 1.5 pm.

The phenomenon observed by Wilkinson *et al.* [11] is not unique. Huffman *et al.* [12] made an analogous set of molybdenum complexes, and determined the structure of $[Mo(Ntol)Cl_3(PEtPh_2)_2]$ (see **3**).

For this d^1 complex they observed the exertion of a *trans* influence on the *trans* chloride. The *trans* chloride had a bond distance to the metal that was 10 pm longer than the bond distances for the equatorial chlorides. Huffman *et al.* [12] noted that there are similar geometric distortions in related d^1 imido complexes. In Table 1 structural data for $[M(NR)Cl_{5-x}(PR'_3)_x]$ complexes are summarised. There is a clear relationship between the d electron configuration of the metal and the length of bond between the metal and the ligand *trans* to the imido group. Additionally, the bending of the equatorial ligands away from the imido group diminishes as the occupancy of the metal d orbitals increases.

This evidence has led some authors [12] to conclude that the magnitude of the *trans* influence exerted by a linear organoimido ligand in pseudooctahedral complexes is markedly dependent upon the electronic configuration of the metal. Thus for d^2 complexes the *trans* influence is negligible; for d^1 complexes the *trans* influence is of the order of 6–10 pm and for d^0 complexes approximately 20–25 pm.

Traditionally the *trans* influence in these π-donor complexes has been thought to be partly due to be a steric/electrostatic phenomenon arising from repulsions between the multiply bonded ligands and the ligands *cis* to it [17]. The structural trends observed by Wilkinson *et al.* [11] contradict this model of the *trans* influence. In a previous study [18], we investigated the relative importance of steric/electrostatic and orbital effects on the *trans* influence. We have concluded that the interactions between the ligands and the metal valence orbitals have a larger rôle to play in determining the extent of the *trans* influence. This has led us to investigate the reasons for the structural trends of $[M(NR)Cl_{5-x}(PR'_3)_x]$ complexes.

2. Computational details

2.1. Molecular orbital calculations

All calculations were based on approximate Density Functional Theory within the Local Density Approxi-

TABLE 1. Structural data for $[Mo(NH)Cl_3(PR_3)_2]^{0,\pm 1}$ complexes

Compound	d_{M-N} (pm)	$d_{M-Cl_{eq}}$ (pm)	$d_{M-Cl_{trans}}$ (pm)	d_{M-P} (pm)	Cl-M-N [a] (°)	P-M-N [a] (°)
$[Mo(Ntol)Cl_3(PEtPh_2)_2]$ [b]	172.5	238.7	248.6	259.9	93.79	90.21
$[Tc(NPh)Cl_3(PPh_3)_2]$ [c]	170.4	241.5	240.4	250.3	92.55	93.20
$[W(NPh)Cl_3(PMe_3)_2]$ [d]	174.2	238.7	244.3	259.0	93.65	90.85
$[W(NPh)Cl_2(PMe_3)_3]$ [d]	175.5	249.1	250.1	247.8	–	–
$[Cr(N^tBu)Cl_3(PEtPh_2)_2]$ [e]	163.4	231.7	238.1	247.9	92.2	99.5
$[Ta(NPh)Cl_3(PEt_3)(THF)]$ [f]	176.5	237.7 [g]	238.5	266.7	98.37	89.11

[a] Average value. [b] ref. 12; [c] ref. 13; [d] ref. 11b; [e] ref. 14; [f] ref. 15. [g] The *trans* influence in this complex is exerted on the THF ligand. The THF distance is normally approximately 215 pm as reported in ref. 16.

mation [19–21], LDA. The exchange factor, α_{ex}, was taken as 0.7 and the correlation potential was that of Stoll *et al.* [22,23] in the parameterization by Vosko *et al.* [24]. The reported calculations were performed utilizing the vectorized version of the HFS–LCAO program suite, ADF, developed by Baerends *et al.* [25,26], and vectorized by Ravenek [27]. The numerical integration procedure applied for the calculations was based on the scheme developed by Boerrigter and Tevelde [28]. The *n*s, *n*p, *n*d, $(n+1)$s and $(n+1)$p shells of molybdenum were represented by a triple-ζ-STO basis set [29,30]. A double-ζ-STO basis set was employed for the *n*s and *n*p shells of the main group elements. For nitrogen, this basis was augmented by a single 3d STO function, and for hydrogen a 2p STO function was used for polarization. The calculations for all the molecules were performed twice. The first set of calculations employed an unpolarized basis set on phosphorus, while the second set included a single 4d STO function as polarization. For all atoms electrons in lower shells were considered as core and treated according to the method of Baerends *et al.* [25]. An auxiliary set [31] of s, p, d, f and g STO functions, centered on all nuclei, was used in order to fit the molecular density and present Coulomb and exchange potentials accurately in each SCF cycle. The total energy of the system was calculated according to the following equation:

$$E = E_{HFS} + E_c + E_x^{NL} + E_c^{NL} \quad (1)$$

Here E_{HFS} is the total statistical energy expression for the Hartree–Fock–Slater method, while E_c, E_x^{NL} and E_c^{NL} are additional correction terms. The first correction term E_c is a correlation potential for electrons of different spins in Vosko's parameterization. The second term E_x^{NL} is a non-local exchange correction proposed by Becke [32]. Finally, E_c^{NL} is a non-local correction to the correlation, proposed by Perdew [33].

2.2. Energy decomposition scheme and bond energies

The bond energies presented in this paper were evaluated according to the generalized transition method developed by Ziegler and Rauk [34]. In addition this method decomposes the total energy of a system into steric and electronic components, allowing for a quantitative energetic analysis of the orbital interactions. The method has been applied successfully to a variety of transition metal complexes and has been reviewed recently [35]. All the bond energy calculations included gradient corrections developed by Becke and Perdew.

2.3. Geometry optimizations

All the calculations were performed in C_{2v} symmetry. This is not an unreasonable limitation since most of the molecules have been structurally characterized as having approximate C_{2v} symmetry. Full optimizations within C_{2v} symmetry were performed for each molecule. The geometry optimization procedure was based on the method developed by Versluis and Ziegler [36]. The geometries were optimized without including non-local gradient corrections, but it has been shown [37] that the effect of non-local gradient corrections on geometry optimizations is negligible.

3. Results and discussion

3.1. Geometries of $[Mo(NH)Cl_3(PR_3)_2]^{0,\pm 1}$ complexes

We have optimized the geometries of three $[Mo(NH)Cl_3(PR_3)_2]^{0,\pm 1}$ complexes (R = H, Me and F) with d^0, d^1 and d^2 electronic configurations, corresponding to Mo^{VI}, Mo^{V} and Mo^{IV} oxidation states respectively. The calculated structural data for these compounds, based on the geometric parameters shown in Fig. 2, are given in Table 2. The ligands PH_3, PMe_3 and PF_3 were chosen to represent varying degrees of phosphine σ-donor and π-acceptor abilities.

TABLE 2. Calculated geometric data for $[Mo(NH)Cl_3(PR_3)_2]^n$, where R = H, Me and F and $n = -1$, 0 or 1

	d_{M-N} (pm)	d_{M-P} (pm)	$d_{M-Cl_{eq}}$ (pm)	$d_{M-Cl_{trans}}$ (pm)	d_{P-X} (pm)	d_{N-H} (pm)	α (°)	β (°)
$[Mo^{VI}(NH)Cl_3(PH_3)_2]^-$	174.0	244.7	256.2	251.4	147.6	103.7	91.47	90.36
$[Mo^{VI}(NH)Cl_3(PMe_3)_2]^-$	174.1	254.6	249.7	255.8	171.2	102.4	91.16	90.33
$[Mo^{VI}(NH)Cl_3(PF_3)_2]^-$	173.4	253.8	251.3	243.4	166.8	102.6	91.51	90.71
$[Mo^{V}(NH)Cl_3(PH_3)_2]$	173.6	250.2	244.9	256.1	147.1	103.6	93.01	91.2
$[Mo^{V}(NH)Cl_3(PMe_3)_2]$	173.8	258.2	240.1	252.3	170.3	103.7	93.21	91.45
$[Mo^{V}(NH)Cl_3(PF_3)_2]$	173.7	257.4	238.2	244.6	164.5	103.6	92.89	92.22
$[Mo(NH)Cl_3(PH_3)_2]^+$	173.9	253.1	235.6	243.4	145.6	105.0	93.32	87.92
$[Mo(NH)Cl_3(PMe_3)_2]^+$	174.1	262.8	236.4	249.3	168.2	104.9	93.97	93.01
$[Mo(NH)Cl_3(PF_3)_2]^+$	174.0	263.4	229.3	239.2	161.2	104.9	93.39	92.18

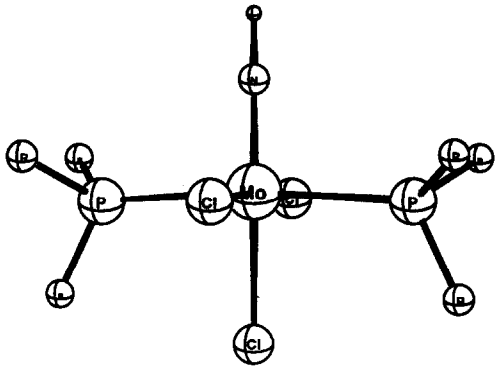

α = Cl - Mo - N

β = P - Mo - N

Fig. 2. Geometrical parameters of the $[Mo(NH)Cl_3(PR_3)_2]^{0,\pm 1}$ complexes.

Firstly let us consider the data for the $[Mo(NH)Cl_3(PR_3)_2]^{\pm 1}$ complexes. For the Mo^{VI} complex, with a d^0 configuration, the imido group exerts a strong *trans* influence on the axial chloride ligand. The $Mo-Cl_{trans}$ bond distance is longer than the $Mo-Cl_{eq}$ bonds. Additionally, the equatorial ligands are bent away from the imido group. The angular distortion of the phosphines is slightly greater than that for the chloride ligands. Reducing the metal to the Mo^{IV} oxidation state results in a change in the geometry of the complex. It appears that the imido group no longer exerts a *trans* influence on the axial chloride, since the $Mo-Cl_{trans}$ bond is now shorter than the bonds between molybdenum and the equatorial chloride ligands. In fact, relative to the Mo^{VI} complex, the $Mo-Cl_{eq}$ distances have increased by 18 pm. Interestingly, the bonds between the molybdenum and the phosphines have shortened by 17 pm compared to the Mo^{VI} complex.

The calculated geometric trends with oxidation state presented here, are also observed for the other complexes that we have studied. The data for $[Mo(NH)Cl_3(PMe_3)_2]$ and $[Mo(NH)Cl_3(PF_3)_2]$ are given in Table 2. The results in Table 2 are in good agreement with the geometric trends observed experimentally for these complexes (Table 1). What appears to be happening is that the ability of the imido group to exert a *trans* influence on the axial chloride diminishes, with increased metal electronic configuration. Indeed many authors attribute the geometric effects to inherent properties of d^2 systems. However, there are many examples of d^2 oxo, imido and nitrido complexes where a large *trans* influence is observed [38]. Therefore, the geometric trends may not be explained simply as an inherent feature of d^2 systems.

3.2. *Electronic structures of PR_3 ligands*

An understanding of the nature of the bonding of the phosphine ligands, and moreover, the nature of the phosphine valence orbitals used in bonding with transition metal fragments, is necessary to understand the geometric diversity of the $[Mo(NH)Cl_3(PR_3)_2]^{0,\pm 1}$ complexes. There have been numerous theoretical studies of trisubstituted phosphine compounds [37–46]. Our intention is not to repeat these detailed studies but to give a summary of the bonding of these ligands as a preparation the subsequent discussion.

Firstly, we consider PH_3, the simplest of the three phosphines used in this study. The orbital interaction diagram for PH_3 is shown in Fig. 3. The $1a_1$ and 1e orbitals correspond to three σ bonds between the phosphorus and the hydrogens. Above these orbitals lies the $2a_1$ orbital which is non-bonding. This is predominantly composed of an sp* hybrid orbital on phosphorus with minor contributions from the σ orbitals of hydrogen. The sp* hybrid on the phosphorus is directed away from the hydrogen atoms. In effect, this orbital may be regarded as the lone pair orbital of PH_3, and it is through this orbital that the PH_3 group

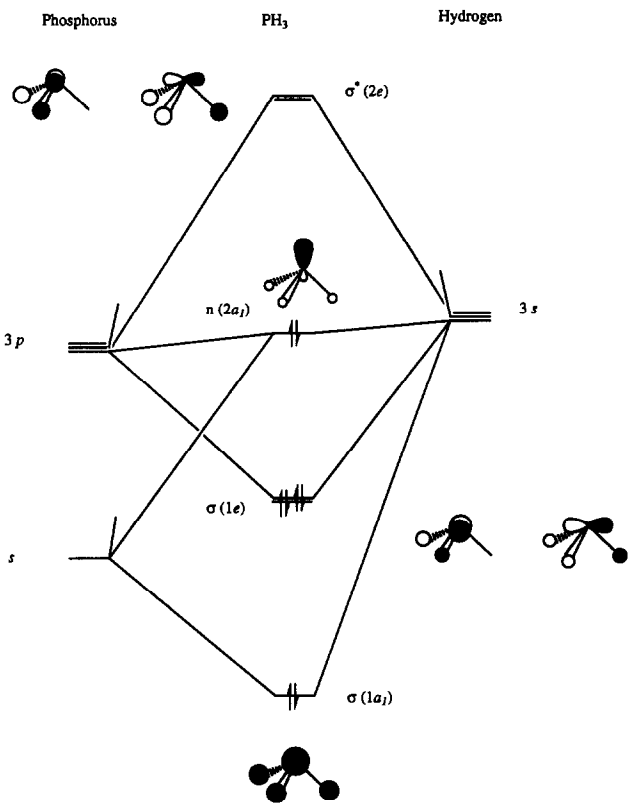

Fig. 3. Fragment orbital diagram of PH_3.

acts as a σ donor ligand. The LUMO of the PH_3 group is doubly degenerate and corresponds to the out of phase equivalent of the lower lying 1e set. Finally, the $3a_1$ orbital (not shown in Fig. 3) lies above the 2e set. Like the 2e orbitals, the $3a_1$ orbital corresponds to a σ^* interaction between the phosphorus and hydrogens. The ordering of the levels found by our calculations is in agreement with Xiao *et al.*'s [47] study of the nature of phosphine frontier orbitals.

The molecular orbital manifolds of PMe_3 and PF_3 are more complicated simply because of the larger basis sets of the methyl and fluorine ligands. Nonetheless, the simplicity of the orbital interaction diagram for PH_3 still holds for PMe_3 and PF_3. Both of these ligands have three low lying orbitals corresponding to σ bonds, a non-bonding orbital centred on phosphorus as the HOMO, and a doubly degenerate unoccupied set corresponding to σ^* interactions between the phosphorus and the ligands. The relative energies of these orbitals for the three phosphines are depicted in Fig. 4, with the corresponding atomic compositions given in Table 3. The energy level orderings are easily rationalized by the relative electronegativities of the ligands: Me < H < F.

Traditionally, the bonding in metal phosphine complexes has been described in terms of σ donation from the phosphine and back donation from the metal [48–49] to phosphorus d orbitals. The σ donating orbital on the phosphine is the non-bonding $2a_1$ orbital of Fig. 3. However, the exact nature of the π acceptor orbital was less clear-cut. Historically, the accepted rationale was that low lying empty 3d orbitals on phosphorus acted as π acceptor orbitals [50,51]. Studies performed by Xiao *et al.* [47] showed the nature of the π acceptor orbitals to be a hybrid of phosphorus d and phosphine σ^* orbitals. Marynick [52] went further by showing that the π acceptor ability of phosphines could be fully accounted for by σ^* orbitals alone. Recently, Pacchioni *et al.* [53] have reported work suggesting that d orbitals enhance the π acceptor ability of phosphines, but the d orbitals merely act as polarization functions.

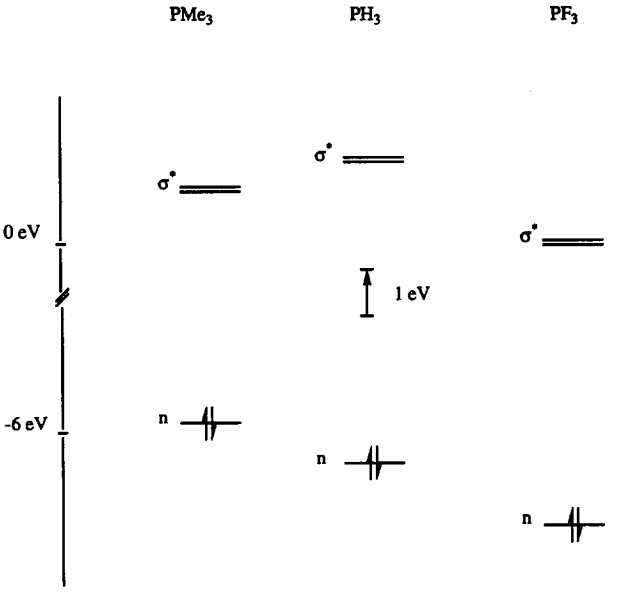

Fig. 4. Frontier energy levels of the PH_3, PMe_3 and PF_3 phosphines.

Indeed, Jacobsen *et al.* [54] have found that the σ^* orbitals of thioethers also act as π acceptors in some complexes. Thus, the current consensus suggests that the σ^* orbitals of phosphines play a more important rôle in back donation in metal-phosphine complexes than the phosphorus 3d orbitals.

The rôle of the $2a_1$ and 2e orbitals of the phosphines (referring to Fig. 3) and the importance of their relative energies in PH_3, PMe_3 and PF_3 complexes is discussed more fully in later sections.

3.3. Analysis of the $[Mo(NH)Cl_3]^{-1}$ fragment

We have optimized the hypothetical $[Mo(NH)Cl_3]^{-1}$ fragment. We had two objectives in mind. Firstly, we wanted to ascertain the geometry of the d^2 $[Mo(NH)Cl_3]^{-1}$ fragment prior to bonding to two phosphine ligands. Secondly, an analysis of the electronic structure of this fragment is useful for the analysis of the phosphine complexes in a later section.

TABLE 3. Atomic compositions of the HOMO and LUMO of the PR_3 ligands [a]

Orbital		Energy (eV)	Atomic compositions						
			P		C		F		H
			2s	2p	2s	2p	2s	2p	1s
PH_3	H	−6.45	0.15	0.59	–	–	–	–	0.09
PH_3	L	1.34	–	0.28	–	–	–	–	0.34
PMe_3	H	−5.85	0.12	0.58	–	0.10	–	–	0.13
PMe_3	L	0.98	–	0.17	–	–	–	–	0.20
PF_3	H	−8.31	0.21	0.28	–	–	–	0.27	–
PF_3	L	0.13	–	0.47	–	–	–	0.21	–

[a] H = HOMO and L = LUMO/unoccupied *e* set.

The optimized structure, together with the calculated geometric parameters, are shown in Fig. 5. The metal–imido bond distance is calculated to be 172 pm, which is typical for second row transition metal–imido bond distances. The length of the Mo–N bond and the linearity of the Mo–N–H angle indicate strong σ and π bonds between the metal and nitrogen. The calculations suggest a *trans* influence being exerted on the chloride ligand *trans* to the imido ligand. This chloride has a bond distance to the metal that is 90 pm longer than the bond distances of the equatorial chlorides. Another characteristic feature of the *trans* influence is an angular distortion of the equatorial chlorides away from the imido group. The angular distortion is not very large in this fragment.

The molecular orbital diagram for the $[Mo(NH)Cl_3]^{-1}$ fragment is shown in Fig. 6. From the metal d orbitals the d_{z^2} and $d_{x^2-y^2}$ orbitals are employed for σ bonding. In C_{2v} symmetry these orbitals both transform as the a_1 irreducible representation, and therefore the metal orbitals involved in σ bonding are hybrids of the d_{z^2} and $d_{x^2-y^2}$ orbitals. The remaining d orbitals are employed in π interactions with the ligand valence orbitals. These $d\pi$ orbitals are symmetrically independent in C_{2v} symmetry. Clearly, the 4s and 4p orbitals of the metal may also take part in orbital interactions, with the 4s and $4p_z$ orbitals participating in σ bonding, the $4p_x$ participating in π bonding and the $4p_y$ orbital participating in both σ and π bonding.

The main σ bonding interactions result in the $1a_1$, $2a_1$, $2b_2$ and $3a_1$ shown in Fig. 6. The $1a_1$ orbital is localized on atoms along the z axis and corresponds to overlap between the σ orbitals of the imido and *trans* chloride ligands with a s/d_{z^2} hybrid on the metal. The s and d_{z^2} hybridization at the metal has resulted in this

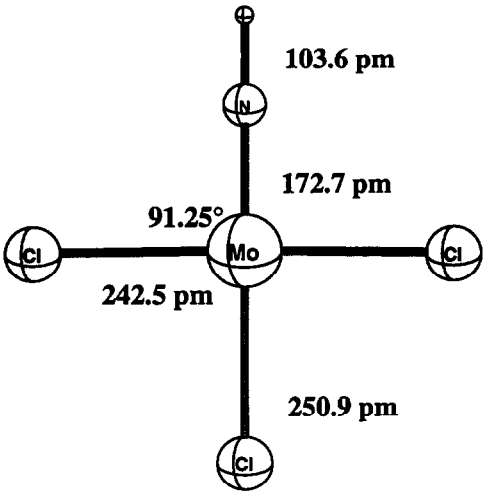

Fig. 5. Optimized geometry of the $[Mo(NH)Cl_3]^{-1}$ fragment.

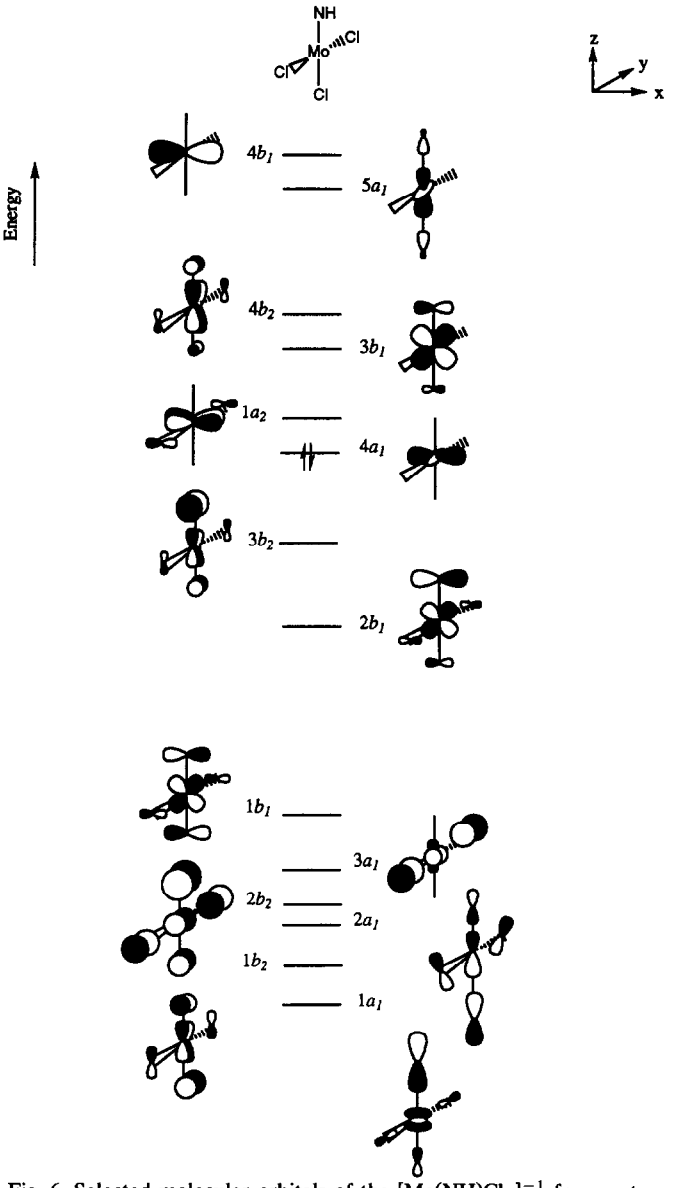

Fig. 6. Selected molecular orbitals of the $[Mo(NH)Cl_3]^{-1}$ fragment.

orbital being directed along the z axis away from the equatorial chlorides. The $2a_1$ orbital corresponds to σ bonding interactions between the metal and the equatorial chloride ligands. Once again, hybridization at the metal is used to maximize overlap with the ligand valence orbitals. A positive admixture of the d_{z^2} orbital into the $d_{x^2-y^2}$ orbital results in the latter being polarized along the y axis towards the chloride σ orbitals. The $2b_2$ and $3a_1$ orbitals involve bonding interactions between the ligands and the metal p_y and p_z orbitals respectively.

The $1b_2$, $1b_1$, $3b_2$ and $2b_1$ orbitals correspond to π interactions in the molecule. The $1b_2$ orbital has a d_{yz} contribution from the metal. Since this orbital is copla-

nar with the ligand plane, there are contributions from all the ligands to this molecular orbital. All the orbital interactions are in-phase, resulting in this orbital being the lowest lying π molecular orbital. The $1b_1$ orbital represents π bonding interactions mainly between the imido and *trans* chloride ligands. This orbital does not benefit from equatorial chloride contributions to the same extent as the $1b_2$ orbital, and therefore lies higher in energy. The $3b_2$ and $2b_1$ orbitals are very similar to the $1b_1$ and $1b_2$ orbitals. They differ in the magnitude of the contribution from the imido π orbitals, and also because these orbitals are out-of-phase with respect to metal–equatorial chloride bonding. The out-of-phase contributions from the equatorial chlorides result in the relative ordering of the $3b_2$ and $2b_1$ orbitals shown in Fig. 6.

The frontier orbitals correspond to non-bonding and antibonding interactions between the metal and the ligand valence orbitals. There are two points to note about the frontier orbitals. Firstly, the $4a_1$ orbital (HOMO) is hybridized away from the equatorial chlorides towards the sites occupied by the phosphine ligands in the $[Mo(NH)Cl_3(PR_3)_2]^{0,\pm 1}$ complexes. Secondly, the high lying $4b_1$ orbital, which is mainly localized on the p_x orbital of the metal, is also suitably oriented to overlap well with the phosphine ligands in the $[Mo(NH)Cl_3(PR_3)_2]^{0,\pm 1}$ complexes.

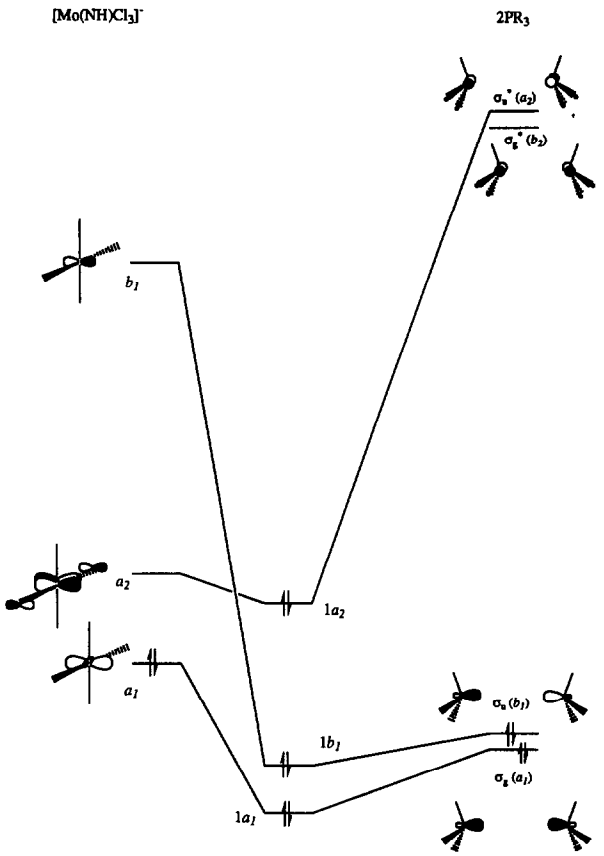

Fig. 7. Selected molecular orbitals of $[Mo(NH)Cl_3(PR_3)_2]^{0,\pm 1}$.

3.4. *Electronic structures of* $[Mo(NH)Cl_3(PR_3)_2]^{0,\pm 1}$ *complexes*

In the previous sections the electronic structures of $[Mo(NH)Cl_3]^{-1}$ and PR_3 fragments were discussed. Now we shall discuss how the frontier orbitals of these fragments interact to produce the molecular orbitals of the parent $[Mo(NH)Cl_3(PR_3)_2]^{0,\pm 1}$ complexes. For the purposes of the discussion we restrict ourselves to the interactions between the PH_3 fragments and the $[Mo(NH)Cl_3]^{-1}$ fragment. The nature of the frontier orbitals of the phosphines are very similar, and so the discussion may readily be applied to the other phosphines studied in these calculations.

The interaction between the fragment orbitals is depicted in Fig. 7. On the right hand side are the linear combinations of the frontier orbitals of the two phosphine groups. Essentially, the σ frontier orbitals of the phosphine fragment dominate its orbital interactions with other fragments. There are two symmetry adapted linear combinations of the phosphine σ orbitals. These are labelled $\sigma_g(a_1)$ and $\sigma_u(b_1)$ for convenience. In addition the unoccupied σ^* orbitals of the phosphine groups are included. The appropriate linear combinations are labelled $\sigma_g^*(a_2)$ and $\sigma_u^*(b_2)$.

The metal fragment frontier orbitals are the same as those discussed previously. The strongest interaction between the fragment orbitals is between the σ_g and σ_u orbitals of the phosphines and the $1a_1$ and $1b_1$ orbitals of the metal fragment. These interactions result in four molecular orbitals (**4–7**), shown below. The bonding interactions, **4** and **5**, correspond to donation of electrons from the phosphine σ orbitals to the $1a_1$ and $1b_1$ orbitals of the metal fragment. These molecular orbitals correspond to Mo–P σ bonds. The simplicity of

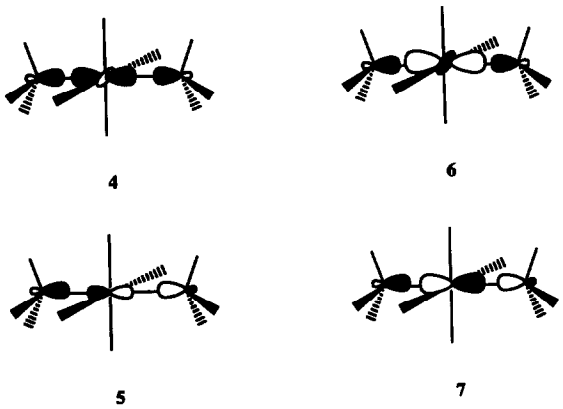

4 **6**

5 **7**

these orbital interactions belies the presence of important subtle interactions between the fragments.

The $1a_2$ orbital of the metal fragment has the same symmetry properties as the $\sigma_g^*(a_2)$ orbitals of the phosphine fragments. The energy difference between these orbitals is large, but nonetheless, there is an overlap between these orbitals to the extent that the $1a_2$ orbital is slightly stabilized (see Fig. 7). If the resulting molecular orbital is occupied, then this interaction represents π donation from the metal to the σ^* orbitals of the phosphine. The π acidity of the phosphines is small in comparison to the σ basicity, but the π acidity is strong enough to influence the geometry of the complex. In a d^2 system, the π acidity of the phosphine provides a means of stabilizing an orbital that is π antibonding with respect to metal chloride interactions. For the complex to fully benefit from this stabilization, the MoNP angle should be as close to 90° as possible. As a consequence, in the d^2 complex the equatorial ligands have angles close to 90°, while for the Mo^{VI} complex, the angles are approximately 94°. Moreover, the Mo^{IV} complex is characterized by short Mo–P bonds and long $Mo–Cl_{eq}$ bonds. This is related to the respective bonding and antibonding nature of the a_2 orbital. The *trans* influence of the imido group alters as the oxidation state of the molybdenum changes. The lengthening of the ligand *trans* to the imido group persists from Mo^{VI} to Mo^{IV} complexes. The angular distortion of the equatorial ligands from an octahedron diminishes with decreasing oxidation state. The decrease in the angular distortion of the equatorial ligands results in the lengthening of the $Mo–Cl_{eq}$ bonds in the Mo^{IV} complex with respect to the Mo^{VI} complex. This gives the incorrect impression that the imido group no longer weakens the $Mo–Cl_{trans}$ bond. Our calculations show that the $Mo–Cl_{trans}$ bond length is virtually unaltered by the change in oxidation state of the metal.

We assert that the geometric differences observed with changing oxidation state is not an inherent property of d^2 systems, as stated by other authors. Rather, the geometric distortions are due to the properties of the equatorial ligands. If there are no π acceptor ligands arranged equatorially to stabilize the d^2 electrons, then the angular distortion will be the same as the d^0 case.

Previously, phosphines have been thought to use 3d orbitals as π accepting orbitals. In a later section the effect of introducing a d polarization function to the phosphorus basis set is investigated. Firstly, the bonding interactions discussed in this section are quantitatively investigated for all the phosphines used in the calculations.

TABLE 4. Bonding energies and decompositions into steric and electronic interactions for the reaction $[Mo(NH)Cl_3]^- + 2PR_3 \rightarrow [Mo(NH)Cl_3(PR_3)_2]^-$ with R = H, Me, and F

All energies are given in kJ mol^{-1}

	Total bonding energy	Steric energy	Orbital interaction
$[Mo(NH)Cl_3]^- + PH_3$	−122.8	517.4	−640.2
$[Mo(NH)Cl_3]^- + PMe_3$	−154.9	684.2	−839.1
$[Mo(NH)Cl_3]^- + PF_3$	−173.2	584.2	−757.4

3.5. Bond analysis and energy decomposition

The generalized transition state method provides not only accurate calculations of total bonding energies [34], but also the possibility of a detail bonding analysis [35,55,56]. The reader is referred to the literature [35] for a detailed description and a list of applications of the transition state method.

For this discussion we shall employ the following expression for the total bonding energy:

$$E = \Delta E^0 + \Delta E_{el} \tag{2}$$

The ΔE^0 term refers to the steric energy change due to bringing the various fragments together to form the molecule. This steric energy term is composed of the following terms:

$$\Delta E^0 = \Delta E_{elst} + \Delta E_{dlxc} + \Delta E_{exrp} \tag{3}$$

The electrostatic term ΔE_{elst} and ΔE_{dlxc} are in general stabilizing while ΔE_{exrp} is in general destabilizing. The ΔE_{dlxc} term refers to the change in correlation energy of the system while the ΔE_{exrp} is an exchange repulsion term that is directly related to destabilizing four-electron two-orbital interactions.

The ΔE_{el} term may also be subdivided into energy terms corresponding to each irreducible representation of the point group of the molecule. Thus for C_{2v} symmetry the electronic energy of the $[Mo(NH)Cl_3(PR_3)_2]^{0,\pm 1}$ complexes is

$$\Delta E_{el} = \Delta E_{A_1} + \Delta E_{A_2} + \Delta E_{B_1} + \Delta E_{B_2} \tag{4}$$

In Table 4 we have decomposed the total bonding energy of $[Mo(NH)Cl_3(PR_3)_2]^-$ into steric and orbital contributions. The most stable bonds are formed with R = F.

To quantify the energetics of the fragment interactions we have decomposed the orbital interaction energy into four irreducible representations of C_{2v} symmetry. We have presented these results in Table 5. This data refers to the orbital interactions between the phosphine ligands and the metal fragment. The interactions considered are σ donation (**8** and **9**) and $d\pi–\sigma^*$ back donation (**10**).

TABLE 5. Decomposition of the orbital interaction energy into contributions from different symmetries for $[Mo(NH)Cl_3]^- + 2PR_3 \rightarrow [Mo(NH)Cl_3(PR_3)_2]^-$ with R = H, Me and F

	a_1 (%)	a_2 (%)	b_1 (%)	b_2 (%)
$ML_4^- + PH_3$	63.1	10.0	25.2	1.7
$ML_4^- + PMe_3$	64.4	8.1	25.4	2.1
$ML_4^- + PF_3$	58.7	14.9	24.1	2.3

TABLE 6. Occupation of $Q(\sigma(a_1))$, $Q(\sigma(b_1))$ and $Q(\pi)$ for the phosphine orbitals in **8**, **9** and **10**; obtained by Mulliken population analysis

	PF_3	PH_3	PMe_3
$Q(\sigma(a_1))$	1.85	1.79	1.74
$Q(\sigma(b_1))$	1.92	1.91	1.93
$Q(\pi)$	0.21	0.11	0.10

It may be seen that for each of the three phosphines studied the $a_1\sigma$ donation interaction is the strongest bonding interaction of all. However, there are variations in the relative proportion of bonding energy accounted for the a_1 interaction for the three complexes. For the PH_3 and the PMe_3 phosphines the contribution from $\sigma(a_1)$ donation from the phosphine lone pairs to the metal fragment represents approximately 65% of the bonding energy. The $\sigma(a_1)$ donation from PMe_3 is slightly higher than that for PH_3. The other σ donation interaction, b_1, is not as stabilizing as the a_1 case. This interaction represents 25.4% of the orbital interaction energy for PMe_3 and 25.2% for PH_3. For the PF_3 system, the σ contributions are slightly smaller. For each phosphine, the contribution from the b_2 interactions is negligible. For each phosphine there is a significant percentage of the orbital interaction energy due to the interaction shown in **10**. The contributions of 8% and 10% for PMe_3 and PH_3 represent a reasonable degree of back donation from the metal to the phosphines. When fluorine is introduced into the phosphorus system the degree of back donation increases to 15% of the total orbital interaction.

The greater percentage of back bonding ability of PF_3 relative to PMe_3 and PH_3 is also illustrated by the relative bonding energies in Table 4 and the Mo–P distances in Table 2. In Table 6 we have given the computed occupations of pertinent fragment orbitals, obtained by a Mulliken population analysis. The σ donation interactions in **8** and **9** have $Q(\sigma(a_1))$ and $Q(\sigma(b_1))$ populations respectively. The $d\pi$-σ^* back donation interaction represented by **10** results in a $Q(\pi)$ population on the σ^* phosphine orbital. Table 6 shows that the PF_3 is a better acceptor of electrons from the metal d_{xy} orbital. We find that the donor ability of the ligands is $PMe_3 > PH_3 > PF_3$ and the acceptor ability is $PF_3 > PH_3 > PMe_3$.

The greater acceptor ability of the PF_3 σ^* orbitals relative to the PH_3 and PMc_3 ligands may be attributed to the greater stability of the PF_3 σ^* orbitals. In addition the P–F σ bond is more polarized towards fluorine than the P–X bond of PH_3 and PMe_3. As a consequence, the P–F σ^* orbital is more localized on phosphorus than the corresponding orbital of PH_3 or PMe_3, thus increasing the σ^*-metal overlap.

Finally, as further evidence for the rôle of the phosphine ligands in determining the geometries of these complexes we have optimized the structure of $[Mo(NH)Cl_3(NH_3)_2]^-$. The optimized structure with relevant structural parameters is shown in Fig. 8. This molecule has a $Mo-Cl_{trans}$ bond length that is longer than the equivalent equatorial distances. Moreover, there is a strong angular distortion of the equatorial ligands from the imido group. This is in total contrast to the structure of the phosphine complexes and is readily explained by the lack of energetically accessible orbitals on the ammonia groups capable of accepting the electrons in the HOMO of the complex. Apart from the energetic inaccessibility of the ammonia σ^*

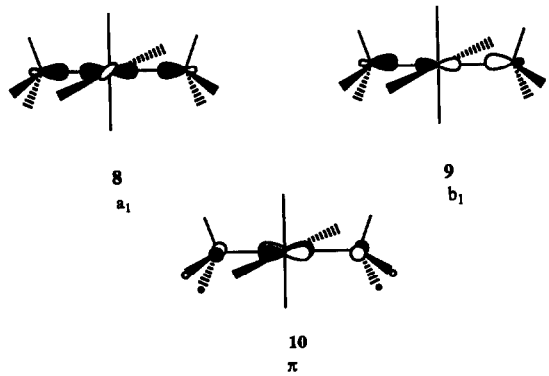

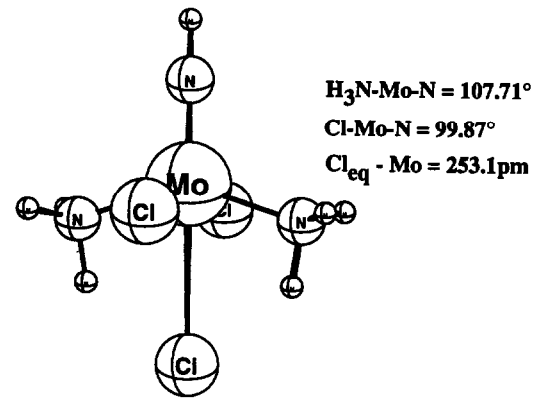

Fig. 8. Optimized structure of $[Mo(NH)Cl_3(NH_3)_2]^-$.

TABLE 7. Decomposition of the orbital interaction energy into contributions from different symmetries for $[Mo(NH)Cl_3]^- + 2PF_3 \rightarrow [Mo(NH)Cl_3(PF_3)_2]^-$ with and without *d* polarization in the phosphorus basis set

	a_1 (%)	a_2 (%)	b_1 (%)	b_2 (%)
With *d* polarization	55.6	18.7	23.9	1.8
Without *d* polarization	58.7	14.9	24.1	2.3

orbitals, these orbitals are more polarized on the hydrogens compared to the equivalent orbitals of PH_3.

3.6. Inclusion of d polarization functions on phosphorus

Recently it has been suggested [57,53] that phosphorus d orbitals may enhance the acceptor abilities of the phosphine σ^* orbitals as shown in **11**.

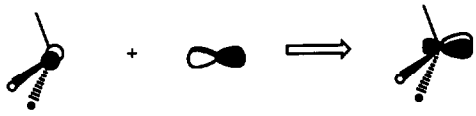

11

The bond energy calculations for the $[Mo(N)Cl_3(PF_3)_2]^-$ complex were repeated with the inclusion of a single d polarization orbital in the phosphorus basis set. The results of these calculations are given in Table 7.

The data in Table 7 indicate that the inclusion of d polarization on phosphorus slightly improves the back donation to the σ^* orbitals, but not to any significant extent, in agreement with previous studies [52,53].

4. Summary and conclusions

The aim of this study was to determine the reasons for the apparent disappearance of the *trans* influence in $[Mo(NH)Cl_3(PR_3)_2]^{0,\pm 1}$ complexes as the occupation of the d orbitals of the metal increases from 0 to 2. The geometries of model d^0, d^1 and d^2 complexes have been optimized and the calculated structural parameters are found to be in agreement with experimentally determined structures. In the d^0 Mo^{VI} complexes the organoimido group exerts a *trans* influence on the *trans* chloride ligand. In addition, the equatorial ligands are bent away from the organoimido group. The LUMO of these complexes is a d_{xy} based orbital on the metal. Occupation of this orbital in the d^2 Mo^{IV} complexes enables a backbonding interaction between the metal d_{xy} orbital and the phosphine σ^* orbital. Consequently, to maximize this overlap the equatorial ligands no longer bend away from the organoimido group. The molecular orbital containing the d^2 electrons is anti-bonding with respect to metal–chloride interactions. This results in a lengthening of the Mo–Cl_{eq} bonds. The Mo–Cl_{trans} bond length is similar in the Mo^{VI}, Mo^V and Mo^{IV} complexes. Thus the *trans* influence with respect to the Mo–Cl_{trans} bond persists in the d^2 complexes but is obscured by the lengthened Mo–Cl_{eq} bonds.

For the Mo^{IV} complexes, the Mo–P bond strength decreases along the series PF_3, PMe_3 and PH_3. The inclusion of d orbitals into the phosphorus basis set slightly increases the interaction between the metal and the phosphines. These results are another illustration of Marynick's findings that the π-acceptability of the phosphines may be attributed to phosphine σ^* orbitals [52]. Inclusion of d polarization orbitals are found to increase the interactions as suggested by Pacchioni *et al.* [49] but only to a small extent.

This study has provided a further illustration of the dominance of orbital interactions in determining geometrical distortions in complexes with the metal bonded to a strong π donor.

Acknowledgements

We thank the AFOSR for financial support. PDL expresses his gratitude to the British Council for a scholarship. We are very grateful to Professor Tom Ziegler for the use of his computing facilities and for many helpful discussions.

References

1 A.O. Chong, K. Oshima and K.B. Sharpless, *J. Am. Chem. Soc., 99* (1977) 3420.
2 D.W. Patrick, L.K. Truesdale, S.A. Biller and K.B. Sharpless, *J. Org. Chem., 43* (1978) 2628.
3 J. Kress, M. Wesolek, J.-P. Le Ny and J.A. Osborn, *J. Chem. Soc., Chem. Comm.,* (1981) 1039.
4 D. Mansuy, P. Battioni and J.P. Mahy, *J. Am. Chem. Soc., 104* (1982) 4487.
5 D.M.-T. Chan, W.C. Fultz, W.A. Nugent, D.C. Roe and T.H. Tulip, *J. Am. Chem. Soc., 107* (1985) 251.
6 A. Pidcock, R.E. Richards and L.M. Venanzi, *J. Chem. Soc., A,* (1966) 1707.
7 (a) T.G. Appleton, H.C. Clark and L.E. Manzer, *Coord. Chem. Rev., 10* (1973) 335; (b) E.M. Shustorovich, M.A. Porai-Koshits and Yu.A. Buslaev, *Coord. Chem. Rev., 17* (1975) 1.
8 Y.K. Syrkin, *Izv. Akad. Nauk SSSR, Otd. Khim. Nauk* (1948) 69.
9 (a) C.H. Langford and H.B. Gray, *Ligand Substitution Processes,* Benjamin, New York, 1985; (b) R. McWeeney, R. Mason and A.D.C. Towl, *Disc. Faraday Soc., 47* (1969) 20.
10 J.K. Burdett and T.A. Albright, *Inorg. Chem. 18* (1979) 2112.
11 (a) A.A. Danopoulus, C. Redshaw, A. Vaniche, G. Wilkinson, B. Hussain-Bates and M.B. Hursthouse, *Polyhedron 12* (1993) 1061; (b) D.C. Bradley, M.B. Hursthouse, K.M.A. Malik, A.J. Nielson and R.L. Short, *J. Chem. Soc., Dalton Trans.,* (1983) 2651.
12 C.Y. Chou, J.C. Huffman and E.A. Maatta, *Inorg. Chem., 25* (1986) 822.
13 T. Nicholson, A. Davison and A.G. Jones, *Inorg. Chim. Acta, 51* (1991) 187.

14 A.A. Danopoulus, B. Hussain-Bates, M.B. Hursthouse, W.-H. Leung and G. Wilkinson, *J. Chem. Soc., Chem. Commun.*, (1990) 1678.
15 M.R. Churchill and H.J. Wasserman, *Inorg. Chem., 21* (1982) 223.
16 F.A. Cotton and D.W.T. Hall, *Inorg. Chem., 17* (1978) 3525.
17 B.R. Ascroft, G.R. Clark, A.J. Nielson and C.F. Rickard, *Polyhedron, 5* (1987) 2081.
18 P.D. Lyne and D.M.P. Mingos, in preparation.
19 O. Gunnarsson and I. Lundquist, *Phys. Rev., B10* (1974) 1319.
20 O. Gunnarsson and I. Lundquist, *Phys. Rev., B13* (1976) 4274.
21 O. Gunnarsson, M. Johnson and I. Lundquist, *Phys. Rev. B20* (1979) 3136.
22 H. Stoll, C.M.E. Pavlidou and H. Preuss, *Theor. Chim. Acta, 49* (1978) 143.
23 H. Stoll, E. Golka and H. Preuss, *Theor. Chim. Acta, 55* (1980) 29.
24 S.J. Vosko, M. Wilk and M. Nusair, *Can. J. Phys., 58* (1980) 1200.
25 E.J. Baerends, D.E. Ellis and P. Ros, *Chem. Phys., 2* (1973) 41.
26 E.J. Baerends, Ph.D. Thesis, Free University, Amsterdam, 1975.
27 W. Ravenek, in H.J.J. Riele, Th.J. Dekker and H.A. van de Vorst (eds.), *Algorithms and Applications on Vector and Parallel Computers* Elsevier, Amsterdam, 1987.
28 P.M. Boerrigter, G. te Velde and E.J. Baerends, *Int. J. Quantum Chem., 33* (1988) 87.
29 G.J. Snijders, E.J. Baerends and P. Vernooijs, *At. Nucl. Data Tables, 26* (1982) 483.
30 P. Vernooijs, G.J. Snijders and E.J. Baerends, *Slater Type Basis Functions for the Whole Periodic System,* Internal report, Free University of Amsterdam, 1981.
31 J. Krijn and E.J. Baerends, *Fit Functions in the HFS-method,* Internal report, Free University of Amsterdam, 1984.
32 A.D. Becke, *J. Chem. Phys., 84* (1986) 4524.
33 J.P. Perdew, *Phys. Rev., B33* (1986) 8822.
34 T. Ziegler and A. Rauk, *Theo. Chim. Acta, 44* (1977) 1.
35 T. Ziegler, *A General Energy Decomposition Scheme for the Study of Metal-Ligand Interactions in Complexes, Clusters and Solids,* NATO ASI, C378, 1992.
36 L. Versluis and T. Ziegler, *J. Chem. Phys., 88* (1988) 322.
37 L. Fan and T. Ziegler, *J. Chem. Phys., 95* (1991) 7401.
38 W.A. Nugent and J.M. Mayer, *Metal Ligand Multiple Bonds,* Wiley, New York, 1988.
39 S. Rothenberg, R.H. Young and H.F. Schaefer, *J. Am. Chem. Soc., 92* (1970) 3243.
40 J.D. Petke and J.L. Whitten, *J. Chem. Phys., 59* (1973) 4855.
41 J.G. Norman, *J. Chem. Phys., 61* (1974) 4630.
42 M.F. Guest, I.H. Hillier and V.R. Saunders, *J. Chem. Soc., Faraday Trans., 2* (1972) 867.
43 R. Moccia, *J. Chem. Phys., 40* (1964) 2176.
44 B.D. Boyd and W.N. Lipscomb, *J. Chem. Phys., 46* (1967) 910.
45 J.M. Lehn and B.J. Munsh, *J. Chem. Soc., Chem. Comm.* (1969) 1327.
46 I.A. Topol, A.V. Kondratenko, L.N. Mazalov, G.N. Dolenko and S.A. Chesnyi, *J. Struct. Chem., 22* (1981) 161.
47 S.-Y. Xiao, W.C. Trogler, D.E. Ellis and Z. Berkovitch-Yellin, *J. Am. Chem. Soc., 105* (1983) 7033.
48 M.J.S. Dewar, *Bull. Soc. Chem. Fr., 18* (1951) C71.
49 J. Chatt and L.A. Duncanson, *J. Chem. Soc.*, (1953) 2939.
50 F.A. Cotton and G. Wilkinson, *Advanced Inorganic Chemistry*, Wiley-Interscience, New York, 1988.
51 J. Huheey, *Inorganic Chemistry,* Harper and Row, New York, 1983.
52 D.S. Marynick, *J. Am. Chem. Soc., 106* (1984) 4064.
53 G. Pacchioni and P.S. Bagus, *Inorg. Chem., 31* (1992) 4391.
54 H. Jacobsen, H.-B. Kraatz, T. Ziegler and P.M. Boorman, *J. Am. Chem. Soc., 114* (1992) 7851.
55 T. Ziegler and A. Rauk, *Inorg. Chem., 18* (1979) 1558.
56 T. Ziegler and A. Rauk, *Inorg. Chem., 18* (1979) 1755.
57 A.G. Orpen and N.G. Connelly, *J. Chem. Soc., Chem. Comm.*, (1985) 1310.